

Metastable Prepores in Tension-Free Lipid Bilayers

Christina L. Ting,¹ Neha Awasthi,^{2,3} Marcus Müller,^{4,*} and Jochen S. Hub^{2,3,†}

¹*Sandia National Laboratories, Albuquerque, New Mexico 87185, USA*

²*University of Goettingen, Institute for Microbiology and Genetics, 37077 Göttingen, Germany*

³*Göttingen Center for Molecular Biosciences, 37077 Göttingen, Germany*

⁴*University of Goettingen, Institute for Theoretical Physics, 37077 Göttingen, Germany*



(Received 31 October 2017; published 23 March 2018)

The formation and closure of aqueous pores in lipid bilayers is a key step in various biophysical processes. Large pores are well described by classical nucleation theory, but the free-energy landscape of small, biologically relevant pores has remained largely unexplored. The existence of small and metastable “prepores” was hypothesized decades ago from electroporation experiments, but resolving metastable prepores from theoretical models remained challenging. Using two complementary methods—atomistic simulations and self-consistent field theory of a minimal lipid model—we determine the parameters for which metastable prepores occur in lipid membranes. Both methods consistently suggest that pore metastability depends on the relative volume ratio between the lipid head group and lipid tails: lipids with a larger head-group volume fraction (or shorter saturated tails) form metastable prepores, whereas lipids with a smaller head-group volume fraction (or longer unsaturated tails) form unstable prepores.

DOI: [10.1103/PhysRevLett.120.128103](https://doi.org/10.1103/PhysRevLett.120.128103)

Lipid membranes define cellular boundaries and are involved in many cellular processes, several of which include the formation or closure of aqueous pores in the membrane. Key functions such as endocytosis and exocytosis, synaptic function, and viral entry into host cells require the opening or closing of pores [1–4]. Antimicrobial peptides kill the cell by forming pores in the bacterial membrane [5]. Apart from such natural processes, membrane pores have found biotechnological and medical applications. For instance, pores induced by electric pulses during a method termed electroporation allow the cellular uptake of drugs, vaccines, or genes (see Ref. [6] and references therein). Understanding and manipulating these processes therefore requires an understanding of membrane pore formation.

One might expect that once the stress on a membrane is removed, the pore simply closes. This scenario, however, is not always observed in electrophysiological or tension experiments. Instead, long-living membrane defects, so-called metastable prepores, were reported nearly forty years ago [7–12]. In experiments, metastable prepores were indirectly revealed by memory effects [7,12] and by flickering conductive events within the lifetime of the prepoire [11]. Hence, a hypothetical free-energy landscape involving a barrier between an intact membrane and the prepoire has been discussed repeatedly [7,12,13], but only very recently—first by MD simulations [14], and later by an elastic theory [15]—has the concomitant free energy been explored.

In this Letter, we determine the conditions for metastable prepores using two complementary methods: (i) potential of mean force (PMF) calculations along a recently

proposed reaction coordinate for pore formation [14] computed with atomistic molecular dynamics (MD) simulations, and (ii) a minimal, coarse-grained (CG) model studied by self-consistent field theory (SCFT) and the string method [16]. We focus on the initial molecular rearrangements of the lipids away from their unperturbed configuration in a planar membrane to a hydrophilic, head-lined pore. These rearrangements are not captured by the classical nucleation theory (CNT), where the free energy of a pore with radius r is defined by

$$F(r) = 2\pi r\sigma - \pi r^2\gamma. \quad (1)$$

Here the first term is the cost of forming the edge of a pore with line tension σ , and the second term quantifies the relief in elastic energy for a membrane under tension γ . For $\gamma > 0$, Eq. (1) predicts a free-energy barrier for rupture $F^* = \pi\sigma^2/\gamma$ at a critical radius $r^* = \sigma/\gamma$, beyond which the pore indefinitely grows and the membrane ruptures. We emphasize that the free-energy barrier at r^* is not the same as the prepoire barrier that we identify in this Letter. Whereas CNT assumes a large, solvent-filled pore with σ corresponding to a macroscopic membrane edge, the early structures during pore nucleation will qualitatively differ, and the free-energy contributions cannot be simply decomposed into the competing edge and elastic terms given in Eq. (1). The difficulty in describing these early molecular rearrangements has posed a significant challenge for resolving the metastable prepoire [13,17], and most prior studies have focused on the later stages of pore formation [13,18–24]. In what follows, we demonstrate that both our recently proposed reaction coordinate [14] and the string

method applied to a coarse-grained (CG) lipid model are able to resolve the molecular determinate for metastable prepore states.

Figures 1(a) and 1(b) show results for the free-energy profile for prepore formation in tensionless bilayers obtained using atomistic PMF and coarse-grained string calculations, respectively. The PMFs are computed along the recently suggested reaction coordinate ξ [14], where ξ corresponds to slices in a membrane-spanning cylinder occupied by polar atoms (see Sec. III B of the Supplemental Material [25] for details). $\xi \approx 0.25$ and $\xi \approx 1$ correspond to an unperturbed bilayer and to a fully formed polar defect, respectively [Figs. 2(a) and 2(c)]. ξ is designed to follow the formation of a continuous polar defect during nucleation, but it does not capture a subsequent expansion of the pore radius, because all pores with larger radii are projected onto $\xi = 1$. The atomistic simulations were conducted with pressure coupling and without applying any external tension. To test the effect of the head-to-tail volume ratio, PMFs are computed for five common phosphatidylcholine (PC) lipids of increasing tail length and tail unsaturation. We find that prepores in membranes with short saturated tails such as DLPC and DMPC [Fig. 1(a), red and black, respectively] are metastable, as evident from the free-energy minimum at $\xi = 1$ and the nucleation barrier at $\xi \approx 0.85$, corresponding to the transition state (TS) of prepore formation [Fig. 2(b)]. Structurally, the TS is characterized by a thin water needle spanning the complete bilayer, a structure that has been observed previously [17]. In contrast, lipids with longer tails (DPPC) and longer, unsaturated tails (POPC and DOPC) [Fig. 1(a), green, blue and orange, respectively] form unstable prepores, as is evident from the absence of a nucleation barrier. Hence, the prepore is metastable only for lipids with a sufficiently

large head-to-tail volume ratio. This finding is corroborated by PMFs for membranes with phosphatidylglycerol (PG) instead of PC head groups (Fig. S1 in the Supplemental Material [25]). Indeed, PMFs for PG membranes with short saturated tails (DLPG and DMPG) exhibit pronounced nucleation barriers; however, owing to the increased volume of PG over PC head groups, PMFs for PG membranes even reveal shallow nucleation barriers for lipids with longer and unsaturated tails (DPPG, POPG, and DOPG). Free simulations starting from an open pore confirm the metastability of pores in DLPC and DMPC, whereas pores in DPPC, POPC, and DOPC rapidly close (Fig. S2 in the Supplemental Material [25]). In line with previous work [17], the free-energy difference between the open pore and the flat membrane also increases with increasing tail length, reflecting that pores in thicker membranes are increasingly unfavorable. Notably, we obtain similar PMFs when using an alternative lipid force field (Fig. S3 in the Supplemental Material [25]).

Figure 1(b) shows the minimum free-energy path (MFEP) for pore formation, as computed with the string method applied to a CG lipid model (see Sec. II of the Supplemental Material [25]). The string method identifies the MFEP by optimizing the reaction coordinate of the transition path connecting any two states on a given free-energy landscape. The MFEP is plotted as a function of the position along the string, where $i = 0$ corresponds to the unperturbed bilayer and $i = 1$ corresponds to the bilayer with a well-defined, hydrophilic pore. The position along the string corresponds to a high dimensional order parameter described by the collective hydrophilic and hydrophobic volume fractions of the CG lipid model. The three curves represent different head-group volume fractions $f_H = N_H/(N_H + 2N_T)$, where f_H is modulated by increasing the number of head monomers from $N_H = 13$ to $N_H = 15$ at a fixed number of tail monomers $2N_T = 28$, yielding membranes with fixed hydrophobic thickness. In line with the PMFs from MD simulations, the MFEPs indicate metastable pores for large head-to-tail volume ratios [Fig. 1(b), magenta and grey] and unstable pores for small head-to-tail volume ratios [Fig. 1(b), brown]. The qualitative agreement between the free-energy profiles obtained from our two methods suggests that (i) the simplified CG model captures the overall physics of pore formation, and (ii) the reaction coordinate used to compute the PMF from atomistic simulations is a reasonable approximation of the true MFEP for pore nucleation.

To further explore the lipid rearrangements during pore formation, in Fig. 2 we show (together with the simulation snapshots) contour plots of the head-group density for the atomistic (middle row) and CG (bottom row) lipids, corresponding to the states highlighted in Fig. 1. The tail and water densities for the atomistic and CG simulations are presented in Figs. S4 and S5 of the Supplemental Material [25]. Additional MD frames for DMPC are

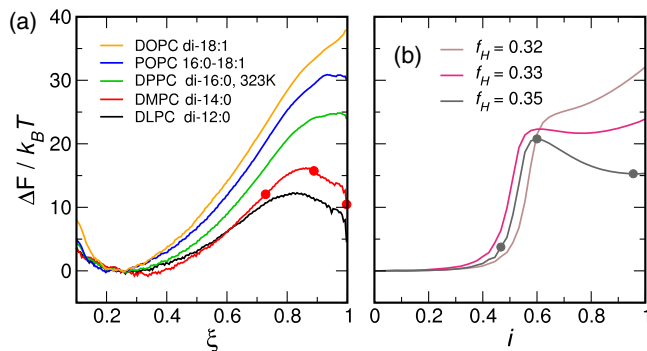


FIG. 1. (a) PMFs of prepore formation from MD simulations in tensionless phosphatidylcholine membranes with increasing tail length and tail unsaturation. The numbers in the legend indicate the structure of the two tails in the format “number of carbon atoms : number of double bonds.” (b) MFEP of prepore formation for a tensionless membrane in coarse-grained SCFT representation, as a function of position i along the string. The three curves correspond to increasing head-group volume fraction: $f_H = N_H/(N_H + 2N_T)$.

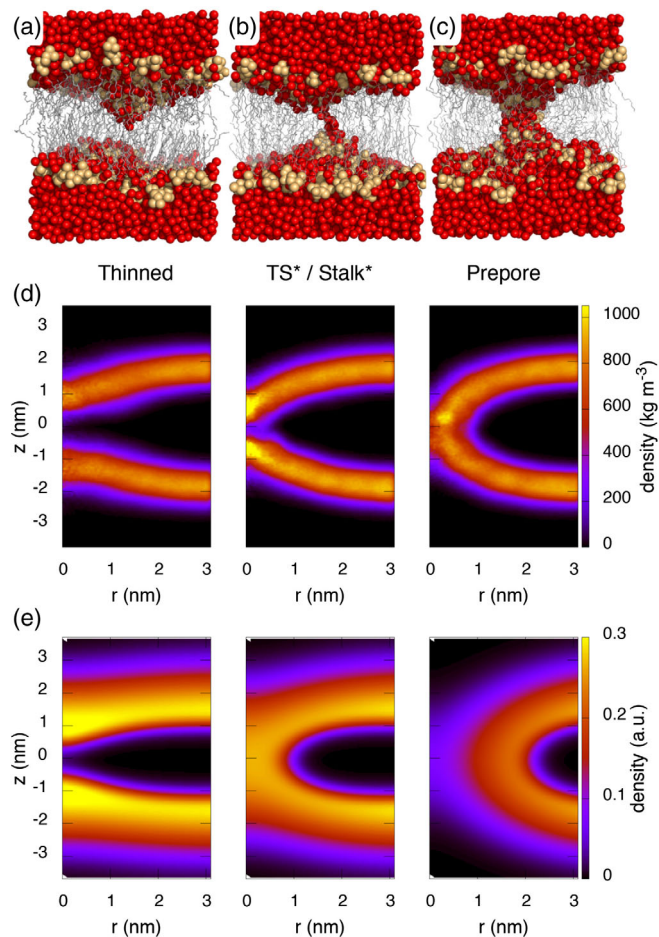


FIG. 2. (a–c) MD simulation snapshots of a DMPC membrane: (a) thinned membrane, (b) transition state of prepore formation, (c) metastable prepore. Water and head-group atoms are shown as red and orange spheres, respectively, and tail atoms are shown as grey sticks. (d) Contour plots in cylindrical coordinates of head-group density in atomistic simulations, shown for states highlighted in the PMF as red dots in Fig. 1(a). (e) Head-group density for the CG simulations for states highlighted along the MFEP as grey dots in Fig. 1(b).

presented in Movie S1 in the Supplemental Material [25]. For $\xi < 0.8$ or $i < 0.55$, the density profiles (Fig. 2, left column) reveal an accumulation of head groups and concomitant thinning of the membrane core. This process is unfavorable, and corresponds to an increase in free energy for all lipids, as shown in Fig. 1. At $\xi \approx 0.85$ or $i \approx 0.6$, the free-energy profiles undergo a notable transition, corresponding to the fusing of hydrated lipid heads from opposing monolayers and exclusion of lipid tails at $r = 0$ to form a hydrophilic stalk through the center of the bilayer (Fig. 2, middle column). In addition, just before the hydrophilic stalk, at $\xi \approx 0.85$ the atomistic simulations reveal a penetration of the membrane by a thin water needle [Fig. 2(b)].

Following the formation of the hydrophilic stalk, for $\xi > 0.85$ or $i > 0.6$, the densities indicate a pinching and

receding of the hydrophilic stalk to form a solvent-filled, head-lined pore, which we call the prepore state (Fig. 2, right column). Whether this process involves an increase or decrease in free energy depends on how well the molecular shape of the lipid is able to accommodate these structural changes. For lipids with shorter, saturated tails [Fig. 1(a), red and black, respectively] or larger head-group volume fractions [Fig. 1(b), magenta and grey, respectively], this process involves a decrease in free energy, and the prepore is hence more stable than the hydrophilic stalk.

Metastability requires, apart from stability with respect to pore resealing, also stability with respect to pore expansion. Because the line tension must be positive for a membrane bilayer to be the stable morphology over a micellar structure [63], i.e., $\sigma > 0$, further expansion of the prepore involves an increase in free energy according to Eq. (1) with $\gamma = 0$. Therefore, we have obtained a metastable prepore state for the lipids with shorter, saturated tails or larger head-group volume fractions. Note that while the barrier for the forward process to form the metastable prepore is on the order of $10\text{--}20k_B T$, the barrier for the reverse process of resealing the prepore only requires overcoming a much smaller barrier of $1\text{--}5k_B T$.

Figure 3(d) explicitly shows the metastability of the prepore in DMPC, by combining (i) the PMF for prepore nucleation starting from a flat membrane, as discussed

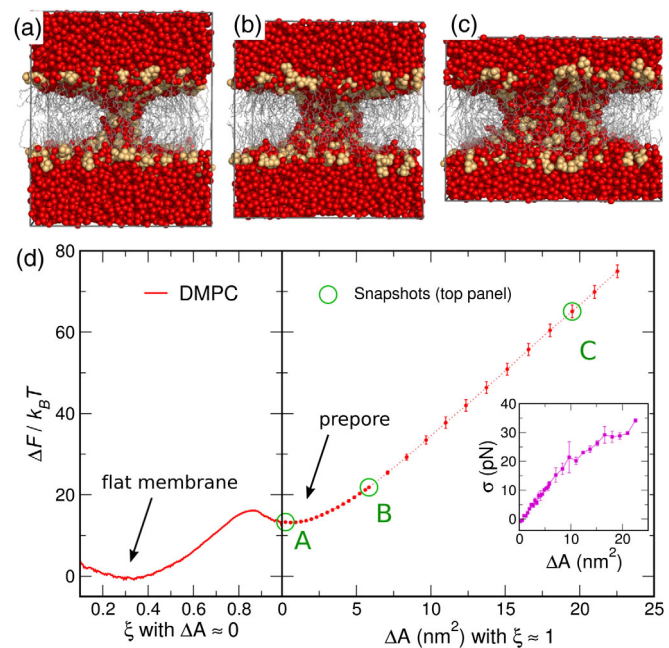


FIG. 3. Free-energy landscape of pore growth following pore nucleation. (a–c) MD snapshots from constant-area simulations with increasing pore size. (d) Left: PMF of prepore formation for DMPC, taken from Fig. 1(a). Right: Free energy with increasing pore size, plotted as a function of the increase of membrane area ΔA at a constant number of lipids, relative to the equilibrium area in the absence of a defect. Green circles refer to the snapshots of panels (a–c).

above [Fig. 3(d), left], with (ii) the PMF for growing the radius of the prepore towards a large, solvent-filled pore [Fig. 3(d), right], as illustrated in MD snapshots in Figs. 3(a)–3(c). Here, the PMF for growing the pore is computed from the anisotropy of the pressure tensor in a series of constant-area simulations (see Sec. III E of the Supplemental Material [25]). The PMF for pore growth, $\Delta F(\Delta A)$, is plotted versus the increase of the simulation box area, ΔA , relative to a flat, unperturbed membrane. As expected for a metastable state, $\Delta F(\Delta A)$ exhibits a quadratic regime for $\Delta A < 7 \text{ nm}^2$. Moreover, the line tension, σ , of the pore edge vanishes for the case of the prepore [Fig. 3(d), inset], and σ increases with increasing pore size to $\sim 30 \text{ pN}$, in reasonable agreement with previous simulations of PC membranes [64]. The pronounced dependence of the line tension on pore size has previously been observed [23] and highlights the breakdown of the CNT assumption of a constant line tension for such small pores. Notably, the shape of the overall free-energy landscape in Fig. 3(d) agrees qualitatively with the landscape hypothesized by Abidor *et al.* nearly forty years ago [7].

We rationalize the metastability of the prepore by packing arguments, since metastability correlates with a large head-to-tail volume ratio f_H (see Fig. 1). Because a large f_H has also been associated with positive spontaneous membrane curvature c_0 [65], it might appear plausible that lipids leading to a larger c_0 could better accommodate the curvature at the pore edge. To test such a hypothesis, we compute the spontaneous curvature c_0 of the CG lipids [66]. For the CG lipids, we find a nearly linear correlation between f_H and c_0 , which could be taken as an argument that c_0 is a determinant for metastability (cf. Fig. S6 of the Supplemental Material [25]). For atomistic lipids, however, no such simple correlation is found; the detailed interactions—and not only the geometrical shape of a lipid—determine c_0 [68]. Therefore, in Fig. S7 of the Supplemental Material [25], we show the region of prepore metastability as a function of f_H for the atomistic and CG lipids.

In contrast to tensionless membranes, membranes under tension exhibit a nucleation barrier for membrane rupture; see Eq. (1). Here, we test whether tension may induce metastability of the prepore—i.e., whether tension may induce a barrier for pore nucleation (in addition to the well-established barrier for rupture). To this end, in Fig. 4(a) we show the MFEP at various tensions for the CG lipid with $f_H = 0.32$, which forms an unstable pore in a tension-free membrane [recall Fig. 1(b), brown]. However, in line with previous work [23], we find that tension does not significantly induce prepore metastability. Instead, tension primarily shifts the transition state for rupture to smaller radii, namely from the radius of the CNT description of a macroscopic pore, r^* , to the radius of the stalk. We find only a narrow parameter range with two barriers separated by a metastable prepore; see Fig. 4(b), where we have

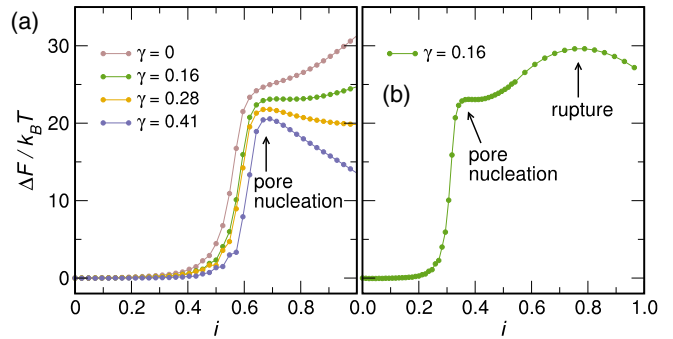


FIG. 4. MFEP for $f_H = 0.32$, as a function of the image number along the string. (a) Different curves correspond to different membrane tensions γ . (b) $\gamma = 0.16$ is extended to show the second barrier for membrane rupture.

expanded the MFEP for $\gamma = 0.16$ to illustrate the additional barrier for membrane rupture. However, the metastable prepore in this case is extremely transient, as the reverse barrier to pore resealing is comparable to the thermal energy scale, $k_B T$. In fact, using tension to stabilize prepores is difficult: as one stabilizes the prepore with respect to the reverse process of resealing, one destabilizes the prepore with respect to the forward process of rupture. This finding seems compatible with the prediction from a membrane-elasticity theory [69]. In atomistic simulations, and in agreement with the results from CG calculations, we find that tension has only a small effect on the metastability of the prepore (see Fig. S8 in the Supplemental Material [25]), providing additional evidence that the lipid shape—and not the tension—determines pore metastability.

CNT assumes (i) the presence of a well-defined pore with constant line tension, σ , and (ii) that the pore radius, r , serves as an appropriate reaction coordinate. We have shown that neither of these assumptions holds during the

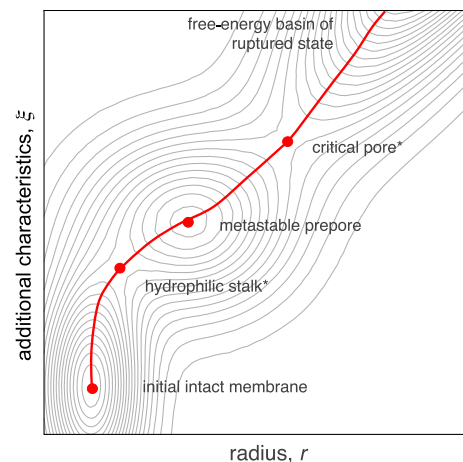


FIG. 5. Schematic of the two-step mechanism involving a metastable prepore. The MFEP (red) is drawn on a hypothetical two-dimensional free-energy landscape. At the early stages, the reaction proceeds in a direction orthogonal to r .

nucleation of a prepore. The string method makes no such assumptions for the reaction coordinate and is hence able to predict MFEPs involving hydrophilic stalks and small, metastable pores. In Fig. 5, we show a schematic of the free-energy landscape for pore formation. Note that the initial stages of the MFEP (red curve) proceed along a direction orthogonal to the radius, r , rationalizing why a simple reaction coordinate, such as the pore radius, fails to capture the initial steps of nucleation. For atomistic simulations, our reaction coordinate [14] is capable of following the early events of pore nucleation, leading to qualitatively similar free-energy profiles as compared to the results from the string method.

To conclude, we have used two complementary methods to derive the physicochemical determinants for metastable prepores. PMF calculations with atomistic MD simulations and the string method combined with SCFT consistently suggest that pore metastability depends primarily on the relative volume ratio between the lipid head group and lipid tails. Membrane tension has a minor effect on stabilizing the prepore state. A theoretical understanding of the stability of the lipid bilayer with respect to pore formation is important for understanding natural processes of biological membranes, as well as for developing lipid compositions that can functionalize vesicles or coatings with controllable and sustained release.

We thank Richard Pastor for sharing updated, unpublished c_0 values of CHARMM36 lipids, and for insightful discussions. C. L. T. acknowledges support from the Alexander von Humboldt Foundation and from Sandia National Laboratories' Laboratory Directed Research and Development (LDRD) program. Sandia National Laboratories is a multimission laboratory managed and operated by National Technology and Engineering Solutions of Sandia, LLC., a wholly owned subsidiary of Honeywell International, Inc., for the U.S. Department of Energy's National Nuclear Security Administration under Contract No. DE-NA0003525, SAND2018-1181 J. M. M. acknowledges support from the Deutsche Forschungsgemeinschaft (DFG), Grant No. SFB 937/A07; N. A. and J. S. H. were supported by the DFG through Grant No. SFB 803/A12. N. A. was additionally supported by a Dorothea-Schötzer fellowship, and J. S. H. was additionally supported by the DFG through Grants No. HU 1971/1-1 and No. HU 1971/4-1.

*mmueller@theorie.physik.uni-goettingen.de

†Present address: Saarland University, Theoretical Physics, Campus E2 6, 66123 Saarbrücken, Germany.
jhub@gwdg.de

[1] R. Jahn, T. Lang, and T. C. Südhof, *Cell* **112**, 519 (2003).
[2] M. Müller, K. Katsov, and M. Schick, *Biophys. J.* **85**, 1611 (2003).

- [3] W. Wu and L.-G. Wu, *Proc. Natl. Acad. Sci. U.S.A.* **104**, 10234 (2007).
[4] H. J. Risselada and H. Grubmüller, *Curr. Opin. Struct. Biol.* **22**, 187 (2012).
[5] C. D. Fjell, J. A. Hiss, R. E. Hancock, and G. Schneider, *Nat. Rev. Drug Discov.* **11**, 37 (2012).
[6] R. A. Böckmann, B. L. De Groot, S. Kakorin, E. Neumann, and H. Grubmüller, *Biophys. J.* **95**, 1837 (2008).
[7] I. G. Abidor, V. B. Arakelyan, L. V. Chernomordik, Y. A. Chizmadzhev, V. F. Pastushenko, and M. R. Tarasevich, *J. Electroanal. Chem.* **104**, 37 (1979).
[8] L. V. Chernomordik, M. M. Kozlov, G. B. Melikyan, I. G. Abidor, V. S. Markin, and Y. A. Chizmadzhev, *Biochim. Biophys. Acta* **812**, 643 (1985).
[9] L. V. Chernomordik, S. I. Sukharev, S. V. Popov, V. F. Pastushenko, A. V. Sokirko, I. G. Abidor, and Y. A. Chizmadzhev, *Biochim. Biophys. Acta* **902**, 360 (1987).
[10] R. W. Glaser, S. L. Leikin, L. V. Chernomordik, V. F. Pastushenko, and A. I. Sokirko, *Biochim. Biophys. Acta* **940**, 275 (1988).
[11] K. C. Melikov, V. A. Frolov, A. Shcherbakov, A. V. Samsonov, Y. A. Chizmadzhev, and L. V. Chernomordik, *Biophys. J.* **80**, 1829 (2001).
[12] E. Evans, V. Heinrich, F. Ludwig, and W. Rawicz, *Biophys. J.* **85**, 2342 (2003).
[13] J. Wohler, W. K. den Otter, O. Edholm, and W. J. Briels, *J. Chem. Phys.* **124**, 154905 (2006).
[14] J. S. Hub and N. Awasthi, *J. Chem. Theory Comput.* **13**, 2352 (2017).
[15] S. A. Akimov, P. E. Volynsky, T. R. Galimzyanov, P. I. Kuzmin, K. V. Pavlov, and O. V. Batishchev, *Sci. Rep.* **7**, 12152 (2017).
[16] W. E. W. Ren, and E. Vanden-Eijnden, *J. Chem. Phys.* **126**, 164103 (2007).
[17] W. D. Bennett, N. Sapay, and D. P. Tieleman, *Biophys. J.* **106**, 210 (2014).
[18] M. Müller and M. Schick, *J. Chem. Phys.* **105**, 8282 (1996).
[19] R. R. Netz and M. Schick, *Phys. Rev. E* **53**, 3875 (1996).
[20] V. Talanquer and D. Oxtoby, *J. Chem. Phys.* **118**, 872 (2003).
[21] Z. J. Wang and D. Frenkel, *J. Chem. Phys.* **123**, 154701 (2005).
[22] W. K. den Otter, *J. Chem. Phys.* **131**, 205101 (2009).
[23] C. L. Ting, D. Appelö, and Z.-G. Wang, *Phys. Rev. Lett.* **106**, 168101 (2011).
[24] A. Grafmüller and V. Knecht, *Phys. Chem. Chem. Phys.* **16**, 11270 (2014).
[25] See Supplemental Material at <http://link.aps.org/supplemental/10.1103/PhysRevLett.120.128103> for a description of computational details, which includes Refs. [26–62].
[26] J. P. M. Jämbeck and A. P. Lyubartsev, *J. Chem. Theory Comput.* **8**, 2938 (2012).
[27] R. Pastor and A. MacKerell, Jr, *J. Phys. Chem. Lett.* **2**, 1526 (2011).
[28] A. Ben-Shaul, I. Szleifer, and W. Gelbart, *Proc. Natl. Acad. Sci. U.S.A.* **81**, 4601 (1984).
[29] A. Ben-Shaul and I. Szleifer, *J. Chem. Phys.* **83**, 3597 (1985).

- [30] I. Szleifer, A. Ben-Shaul, and W. Gelbart, *J. Chem. Phys.* **83**, 3612 (1985).
- [31] T. Zemb and C. Chachaty, *Chem. Phys. Lett.* **88**, 68 (1982).
- [32] J. Charvolin, *J. Chim. Phys. Phys.-Chim. Biol.* **80**, 15 (1983).
- [33] P. van der Ploeg and H. Berendsen, *J. Chem. Phys.* **76**, 3271 (1982).
- [34] P. van der Ploeg and H. Berendsen, *Mol. Phys.* **49**, 233 (1983).
- [35] O. Edholm, H. Berendsen, and P. van der Ploeg, *Mol. Phys.* **48**, 379 (1983).
- [36] M. Müller, K. Katsov, and M. Schick, *J. Polym. Sci., Part B: Polym. Phys.* **41**, 1441 (2003).
- [37] C. Ting and Z.-G. Wang, *Biophys. J.* **100**, 1288 (2011).
- [38] G. H. Fredrickson, *The Equilibrium Theory of Inhomogeneous Polymers* (Oxford University Press, Oxford, 2006).
- [39] K. Hong and J. Noolandi, *Macromolecules* **13**, 964 (1980).
- [40] J. M. H. M. Scheutjens and G. J. Fleer, *J. Chem. Phys.* **83**, 1619 (1979).
- [41] X. Y. Cheng, L. Lin, W. E, P. W. Zhang, and A. C. Shi, *Phys. Rev. Lett.* **104**, 148301 (2010).
- [42] W. H. Li, P. F. Nealey, J. J. de Pablo, and M. Müller, *Phys. Rev. Lett.* **113**, 168301 (2014).
- [43] N. M. Maurits and J. G. E. M. Fraaije, *J. Chem. Phys.* **107**, 5879 (1997).
- [44] E. Reister, M. Müller, and K. Binder, *Phys. Rev. E* **64**, 041804 (2001).
- [45] C. J. Knight and J. S. Hub, *Bioinformatics* **31**, 2897 (2015).
- [46] S. Miyamoto and P. A. Kollman, *J. Comput. Chem.* **13**, 952 (1992).
- [47] B. Hess, *J. Chem. Theory Comput.* **4**, 116 (2008).
- [48] W. F. van Gunsteren and H. J. C. Berendsen, *Mol. Simul.* **1**, 173 (1988).
- [49] G. Bussi, D. Donadio, and M. Parrinello, *J. Chem. Phys.* **126**, 014101 (2007).
- [50] H. J. C. Berendsen, J. P. M. Postma, A. DiNola, and J. R. Haak, *J. Chem. Phys.* **81**, 3684 (1984).
- [51] T. Darden, D. York, and L. Pedersen, *J. Chem. Phys.* **98**, 10089 (1993).
- [52] U. Essmann, L. Perera, M. L. Berkowitz, T. Darden, H. Lee, and L. G. Pedersen, *J. Chem. Phys.* **103**, 8577 (1995).
- [53] M. J. Abraham, T. Murtola, R. Schulz, S. Páll, J. C. Smith, B. Hess, and E. Lindahl, *SoftwareX* **1**, 19 (2015).
- [54] W. L. Jorgensen, J. Chandrasekhar, J. D. Madura, R. W. Impey, and M. L. Klein, *J. Chem. Phys.* **79**, 926 (1983).
- [55] G. M. Torrie and J. P. Valleau, *Chem. Phys. Lett.* **28**, 578 (1974).
- [56] S. Kumar, D. Bouzida, R. H. Swendsen, P. A. Kollman, and J. M. Rosenberg, *J. Comput. Chem.* **13**, 1011 (1992).
- [57] J. S. Hub, B. L. de Groot, and D. van der Spoel, *J. Chem. Theory Comput.* **6**, 3713 (2010).
- [58] C. Rycroft, *Chaos* **19**, 041111 (2009).
- [59] T. Tolpekina, W. Den Otter, and W. Briels, *J. Chem. Phys.* **121**, 8014 (2004).
- [60] B. Hess, *J. Chem. Phys.* **116**, 209 (2002).
- [61] O. Berger, O. Edholm, and F. Jähnig, *Biophys. J.* **72**, 2002 (1997).
- [62] H. J. C. Berendsen, J. P. M. Postma, W. F. van Gunsteren, and J. Hermans, in *Intermolecular Forces*, edited by B. Pullman (D. Reidel Publishing Company, Dordrecht, 1981), pp. 331–342.
- [63] H. Pera, J. M. Kleijn, and F. A. M. Leermakers, *J. Chem. Phys.* **142**, 034101 (2015).
- [64] H. Leontiadou, A. E. Mark, and S. J. Marrink, *Biophys. J.* **86**, 2156 (2004).
- [65] J. Israelachvili, *Intermolecular & Surface Forces*, 2nd ed. (Academic Press, London, 1991).
- [66] A standard method for calculating the spontaneous curvature c_0 involves computing the free energy of an interface in cylindrical coordinates as a function of the curvature $c = 1/r$. The resulting free energy per unit area is fit to the Helfrich Hamiltonian [67], where the coefficients may be used to obtain c_0 .
- [67] W. Helfrich, *Z. Naturforsch.* **28C**, 693 (1973).
- [68] R. Pastor (private communication).
- [69] S. A. Akimov, P. E. Volynsky, T. R. Galimzyanov, P. I. Kuzmin, K. V. Pavlov, and O. V. Batishchev, *Sci. Rep.* **7**, 12509 (2017).